# ELECTRONIC SUPPLEMENTARY INFORMATION

## miR-122 direct detection in human serum by time-gated fluorescence imaging

Emilio Garcia-Fernandez,[a] M. Carmen Gonzalez-Garcia,[a] Salvatore Pernagallo,[b,c] Maria J. Ruedas-Rama,[a] Mario A. Fara,[b] Francisco J. Lopez-Delgado,[b] James W. Dear,[d] Hugh Ilyine,[c] Cristina Ress,[e] Juan J. Díaz-Mochón[b, f-g] and Angel Orte [a] *

(a) *Departamento de Fisicoquimica. Unidad de Excelencia de Química aplicada a Biomedicina y Medioambiente, Facultad de Farmacia, Universidad de Granada, Campus de Cartuja s/n, 18071 – Granada, Spain. * E-mail: angelort@ugr.es*
(b) *DestiNA Genomica S.L., Parque Tecnológico Ciencias de la Salud (PTS), Av. de la Innovación 1, Edificio BIC, Armilla, Granada, Spain.*
(c) *DestiNA Genomics Ltd., 7-11 Melville St, Edinburgh EH3 7PE, United Kingdom.*
(d) *Centre for Cardiovascular Science, University of Edinburgh, The Queen's Medical Research Institute, 47 Little France Crescent, Edinburgh, EH16 4TJ, UK*
(e) *Optoi Microelectronics, Via Vienna n° 8, 38121 – Gardolo, Trento, Italy.*
(f) *GENYO - Centre for Genomics and Oncological Research: Pfizer/University of Granada/Andalusian Regional Government, Av. de la Ilustración, 114, 18016 – Granada, Spain.*
(g) *Departamento de Quimica Farmaceutica y Organica, Facultad de Farmacia, Universidad de Granada, Campus de Cartuja s/n, 18071 – Granada, Spain.*

## Table of contents

# EXPERIMENTAL PART

## E1. Materials

### E1.1. General reagents and stock solutions

Commercially available chemicals were purchased from Sigma Aldrich and were used as received. Working solutions were freshly prepared, using low conductivity milliQ water, prior to each experiment from stock solutions prepared and kept refrigerated at 4°C. The 10 mM phosphate buffer was prepared by mixing the appropriate amounts of $Na_2HPO_4$ and $NaH_2PO_4$ with the pH adjusted to 6.0 using HCl or NaOH 1 M. For the lysis of plasma samples, it was used the Stabiltech Buffer from DESTINA Genomics Ltd. The buffer is based on proprietary combinations of buffering agents, mild detergents, proteinase K and various salts that enhance the extraction of miRs and maintain the stability of the lysed miR-122. Bovine serum albumin (BSA) used for control experiments was commercial powder from Sigma-Aldrich. Q-Sepharose beads (Q-Sph) are crosslinked agarose matrix beads covered at the surface with quaternary amines and were purchased from GE Healthcare Life Sciences. The diameter of the beads ranged from 45 to 165 μm, as detailed by the supplier. Prior to use, Q-Sph was equilibrated. Briefly, 1mL was centrifuged and the supernatant removed. The resin was subsequently washed centrifugally with $H_2O$ (1 mL) once and twice with 10 mM phosphate buffer pH 6 (1 mL), before resuspending in the same buffer (0.5 mL). Immediately before use, the pre-equilibrated Q-Sph suspension was agitated to resuspend the resin beads. SeTau425 was purchased as NHS ester from SETA BioMedicals (USA). As reducing agent in the dynamic chemistry reaction[1], sodium cyanoborohydride ($NaBH_3CN$) was employed. PNA probes (PNA122* and DGL122) as well as the SMART-C-SETau425 (SB-C*), were designed, synthesised and characterized by DestiNA Genomica S.L. (Spain), see below. All synthetic DNA oligomers were purchased in desalted form from Integrated DNA Technologies (IDT).

## E1.2. PNA122* and DGL122 hybridization probes

Two peptide nucleic acid (PNA) probes (PNA122 and DGL122) were synthesized using standard solid phase chemistry on an INTAVIS MultiPep Synthesiser (IntavisAG GmH, Germany) (see Table S1). The N-terminal-SETau425-modified PNA122 (PNA122*) was designed to allow anti-parallel hybridization with synthetic mimic oligomer DNA miR-122 (see Table S2). In contrast, the DGL122 sequence was designed including and terminated with an acetyl-pegylated group and an abasic "blank" site positioned at +13 from their C-terminal end so that post-hybridisation, with the mimic oligomer DNA miR-122 presents a guanine at that position (+13/+15 from the 5'-terminus of mature hsa-miR-122-5p) thereby allowing incorporation of a cytosine into the blank site or *pocket* (Table S2, nucleobases under interrogation via dynamic chemistry labelling, DCL, shown in red).

**Table S1.** Sequence of PNA122* and DGL122 probes.

| Reference | Oligomer sequence (N'–C') | N'-modification |
|---|---|---|
| **PNA122*** | A A C A C C A T T G T C A C A C T C | SETau425 |
| **DGL122** | A A C A C -- A T T G T C A C A C T C | Acetyl-pegylated group |

'--': abase monomer (blank).

**Table S2.** Sequence of single-stranded DNA oligonucleotides, mimicks of target miRs.

| Reference | Oligomer sequence (5'–3') | Length |
|---|---|---|
| **miR-122** | GAGTGTGACAATGGTGTT | 18 |
| **miR-122-22G** | TGGAGTGTGACAATGGTGTTTG | 22 |
| **miR-122-18A** | GAGTGTGACAATAGTGTT | 18 |

'In red': The nucleobase of miR-122 under interrogation via dynamic chemistry.

## E1.3. Synthesis of SETau425-labelled aldehyde cytosine (SB-C*)

Aldehyde-modified cytosine tagged with the SETau425 reporter dye was prepared following the synthetic route described elsewhere[2] and purified by HPLC and characterized by MALDI-TOF mass spectrometry (see Figures S1-S2).

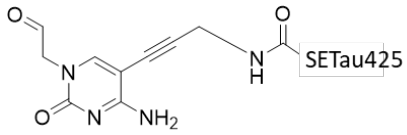


**Figure S1.** Molecular structure of modified cytosine SB-C*

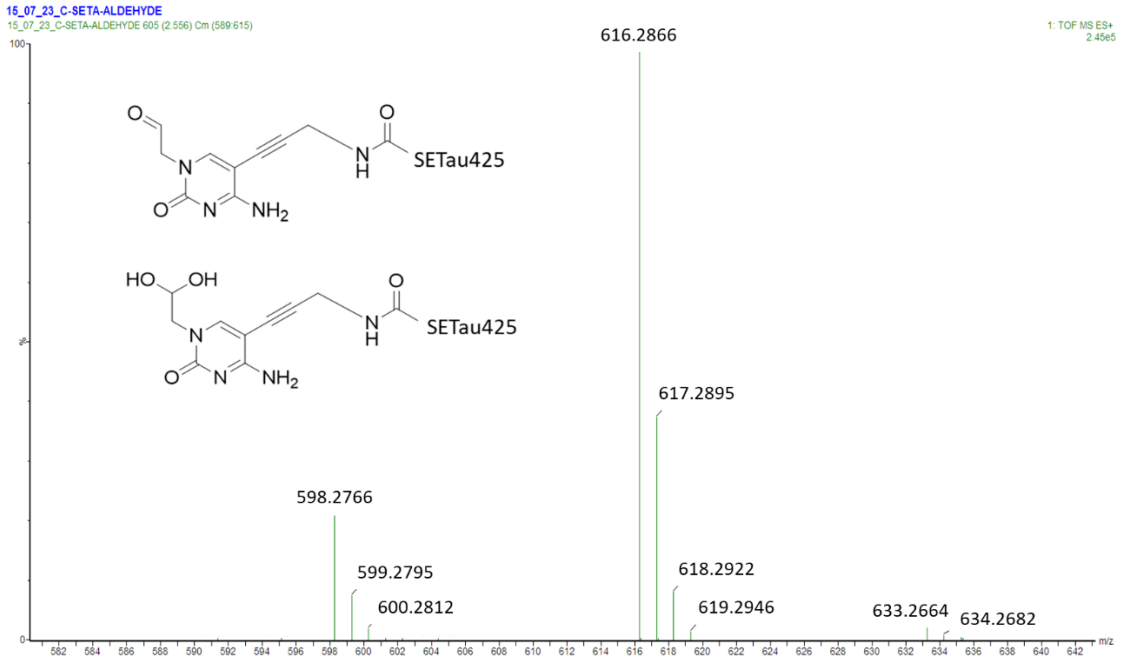


**Figure S2.** MADLI-TOF Mass Spectra of SB-C*. Cation: Chemical Formula: $C_{32}H_{36}N_7O_5^+$; Exact Mass: 598.2772; Molecular Weight: 598.6835. Anion: Chemical Formula: $C_{32}H_{36}ClN_7O_5$; Exact Mass: 633.2466; Molecular Weight: 634.1340.

## E1.4. Blood serum samples

We analysed samples coming from a single patient suffering from drug-induced liver injury (DILI). The adult patient was recruited in a global study called the Markers and Paracetamol Poisoning (MAPP) study,[3] fulfilling the study inclusion criteria: a history of paracetamol overdose, resulting in treatment with intravenous acetylcysteine after evaluation of the treating clinician. Full informed consent was obtained from the participant and ethical approval was given by the South East Scotland Research Ethics Committee and the East of Scotland Research Ethics Committee via the South East Scotland Human Bioresource. The blood sample was taken at the presentation to hospital and it was stored at −80°C as plasma. The patient was affected by an acute liver injury, pre-defined as a peak hospital stay serum alanine transaminase activity (ALT) greater than 100U/L[4].

Human serum sample used as a negative miR-122 control and for spiking experiments was purchased from Sigma Aldrich (H6914 - Human serum from male AB clotted whole blood; USA origin, sterile-filtered).

# E2. METHODS

## E2.1. Methodology for the detection of miR-122 with labelled PNA122* probe

As a first approach, designed to check whether the Q-Sph capturing and subsequent TGI imaging may succeed for detection of miR-122, we employed directly a complementary PNA oligomer (PNA122*, Table S1) labelled with the fluorescent dye of long τ (SETau425). By definition, this methodology does not reach single-nucleotide specificity, and it only should be considered as a proof-of-concept for the viability of the DCL-TGI assay.

The performance of the PNA122*/miR-122 methodology was confirmed by the hybridization of PNA122* with the complementary miR-122 strand (Table S2). Briefly, 33 µL of PNA122* (30 µM), 10 µL of miR-122 (100 µM) and 57 µL of 10 mM phosphate buffer pH 6, were mixed in a 200 µL eppendorf tube. Hybridization was conducted at 41° C for 30 min followed by cooling down slowly at room temperature. The resulting solution with final duplex concentration of 10 µM was diluted to the desired concentration, and subsequently captured with the Q-Sph beads and TG-imaged.

The separation of the PNA122*/miR-122 duplexes was performed by adding 100 µL of pre-equilibrated Q-Sph beads to 100 µL of duplex-containing solution. Solutions were vortexed and incubated at room temperature for 20 min at 1250 rpm. Afterward, solutions were washed three times with 200 µL of buffer and centrifuged for 2 min at 2000 rpm, and the supernatant removed. Finally, the beads were resuspended in 20 µL of buffer before being analysed in TGI imaging.

Chart S1 depicts the whole process for this methodology.

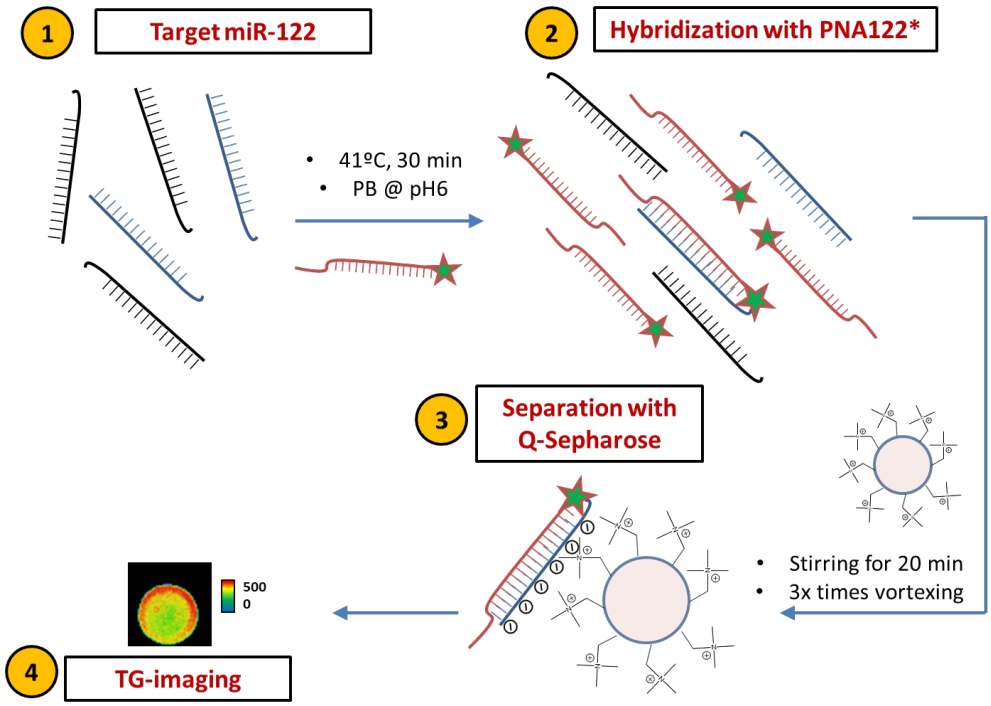


**Chart S1.** PNA122*/miR-122 methodology employed for detection of miR-122 in a single step hybridization and subsequent purification with Q-Sph before TGI imaging.

### E2.2. DCL-TGI assay for the detection of miR-122 with single-base specificity

The labelling via DCL in the DCL-TGI assay was performed by incorporating the SB-C* base upon the hybridization of DGL122 with target miR-122 sequences. Briefly, DGL122 (50 μM), SB-C* (45 μM), $NaBH_3CN$ (2.5mM) and target miR strands (Table S2) to give a final concentration of 1 μM of duplexes, 5μM of SB-C* and 150 mM of $NaBH_3CN$ were added in a single step to a 200 μL eppendorf, vortexed and incubated (41 °C for 30min, thermal cycler). The solution was allowed to slowly cool down at room temperature.

The capturing and separation of the hybridized and labelled DGL122/miR-122 duplexes was performed exactly as described in section E2.1 for the PNA122*/miR-122 methodology.

### E2.4. TGI imaging instrumentation

Fluorescence lifetime (FLIM) and TGI-filtered images were obtained in a MicroTime 200 microscope system (PicoQuant GmbH). The excitation source was a 440-nm pulsed laser (LDH-P-C-440, PicoQuant) controlled by a "Sepia" driver (PicoQuant) to adjust the power and repetition rate to 5 MHz, giving a 200-ns total time-window. The laser powers typically employed were 0.7, 5.3 and 81.1 μW at the photodiode. The excitation pulses were directed into the specimen through a 1.4 NA, 100× oil immersion objective of an IX-71 inverted confocal microscope (Olympus), after being reflected on a 440 DCXR dichroic mirror (Chroma). The fluorescence emission was filtered by a 460LP (AHF/Chroma) cut-off filter, and focused onto a 75-μm pinhole. The fluorescence emission was directed through a 550/50 bandpass filter (Omega Filters) to a single photon avalanche diode SPCM-AQR 14 (Perkin Elmer) able to detect individual photons and sent the corresponding signal to a TimeHarp 200 single photon timing (SPT) module (PicoQuant).

The FLIM and TGI image acquisition was performed taking 10-20 μL of bead-containing solution and placing it over the microscope slide. First, the beads were located and selected with the brigthfield at the oculars of the microscope, and then an initial pre-scan, at very low laser power to avoid photobleaching effects, of an 80×80 $\mu m^2$ area was performed to test the fluorescence intensity of the bead. Then, another scan of the same area at the suitable laser intensity with a 256x256 pixel resolution was recorded. The laser was focused onto different particles and the images of different particles collected. The FLIM images were analyzed and processed using SymphoTime 32 software (PicoQuant). The ensemble image decay was fitted to detect the presence of the SeTau425 fluorescent probe lifetime. Time-gated filtering was applied by selecting just the photons of certain time-window, usually 2 filtering levels: full gate or from 55 ns onwards (time-gated). A previous spatial binning of 5x5 pixels and prehistogramming of 8 temporal channels (for a final resolution of 464 ps/channel) were used to achieve a larger number of counts in each pixel. Later, the intensity images were exported to ImageJ 1.52b software[5] for processing. In brief, first a threshold was applied to remove the background counts and later a pseudocolour scale for intensity was applied (Fig. S3).

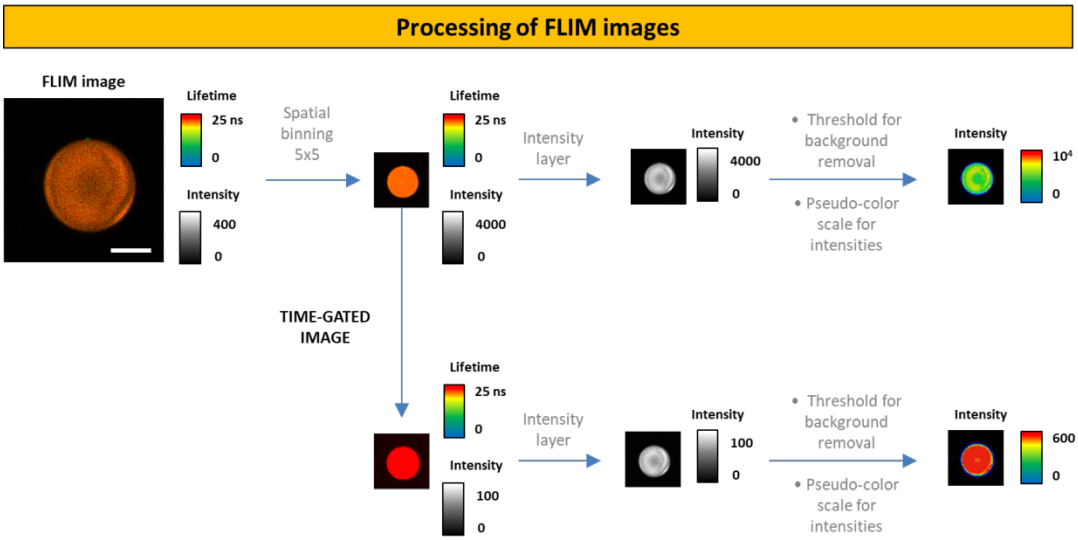


**Figure S3.** Processing of FLIM images into TG intensity images. White scale bar corresponds to 20 µm.

## E2.5. Time-gated filtering of photons

FLIM microscopy takes advantage of time-resolved fluorescence methods since they register both intensity and lifetime of the sample for each interrogated pixel, building up a final image containing this information with spatial resolution. Single photon timing (SPT) permits us to discriminate individual photons depending on the arrival time to the detector. The decay of the fluorescence emission is a random phenomenon and the lifetime of fluorescence, τ, is defined as the time when (100/*e*) % of the total excited molecules has relaxed to the ground state. For each pixel and for the ensemble image we obtain a histogram of intensity (counts) *vs.* arrival time. This is illustrated in figure S4. In SPT mode, we can differentiate short- and long-lived emitting molecules by selecting an appropriate time window (time-gating) subsequently to acquisition. Reconstructing the image only with the photons detected within this time window produces the TG-filtered image.

To illustrate this, we have modelled a hypothetical situation in which we have a fluorescence decay trace that is the sum of three different contributions: an instrument response function (IRF), with an apparent lifetime of 0.5 ns; a short-lived fluorescence emission from the background, with an apparent lifetime of 5 ns; and the fluorescence of the SeTau425 probe, with a 25 ns fluorescence lifetime (Fig. S4). Applying a time window starting *in line a* (from 5 ns onwards), the photons selected will come from both the 5-ns and the 25-ns sources, but discarding IRF photons. If we close the time-window starting now in *line b*, the only source of photons will be the species that emits with a lifetime of 25 ns.

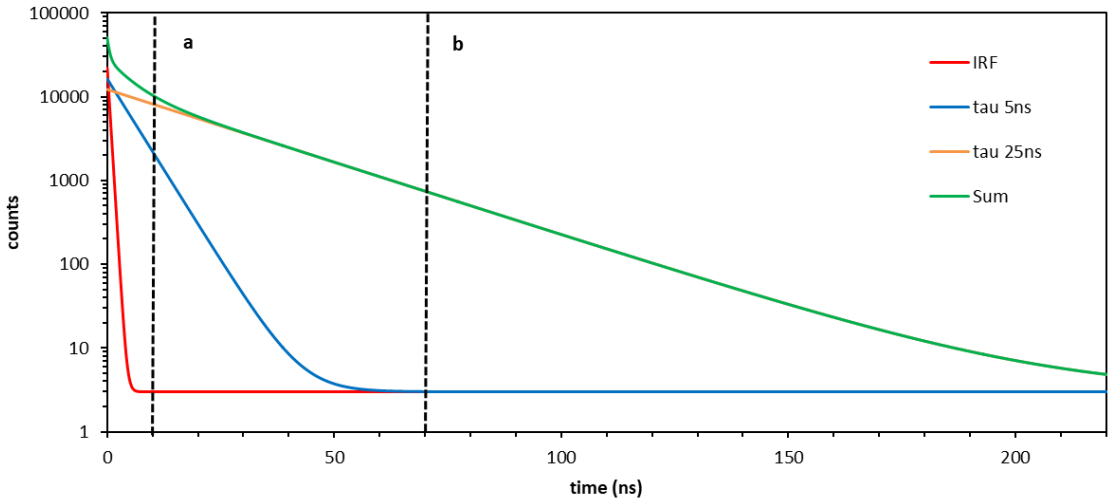


**Figure S4.** Simulated fluorescence decay traces of three different emitters with average lifetime values of 0.5 ns (red), 5 ns (blue), and 25 ns (orange), and the triexponential sum of equal contributions of the three of them (green). The dashed lines (a) and (b) represents time-windows starting in 10ns and 70ns, respectively.

In our particular case, we have a full time-window of 200 ns (5 MHz pulse repetition rate). In figure S5, we show the application of different filtering time-windows for the duplex PNA122*/miR-122 adsorbed over Q-Sph beads, and a control with the Q-Sph beads only. The majority of fluorescence from Q-Sph is detected in times shorter than 55 ns. Therefore, we may exclusively detect fluorescence photons from SeTau425 by filtering out all photons arriving before 55 ns. This filtering causes a big loss of intensity (89%), but we can safely and unequivocally attribute the source of the remaining counts. It is clear that the narrower the detection time-window is, the fewer the number of detected photons is, but in contrast the smaller the contribution from Q-Sph is. The TG images resulting from this filtering process are shown in Figure S6.

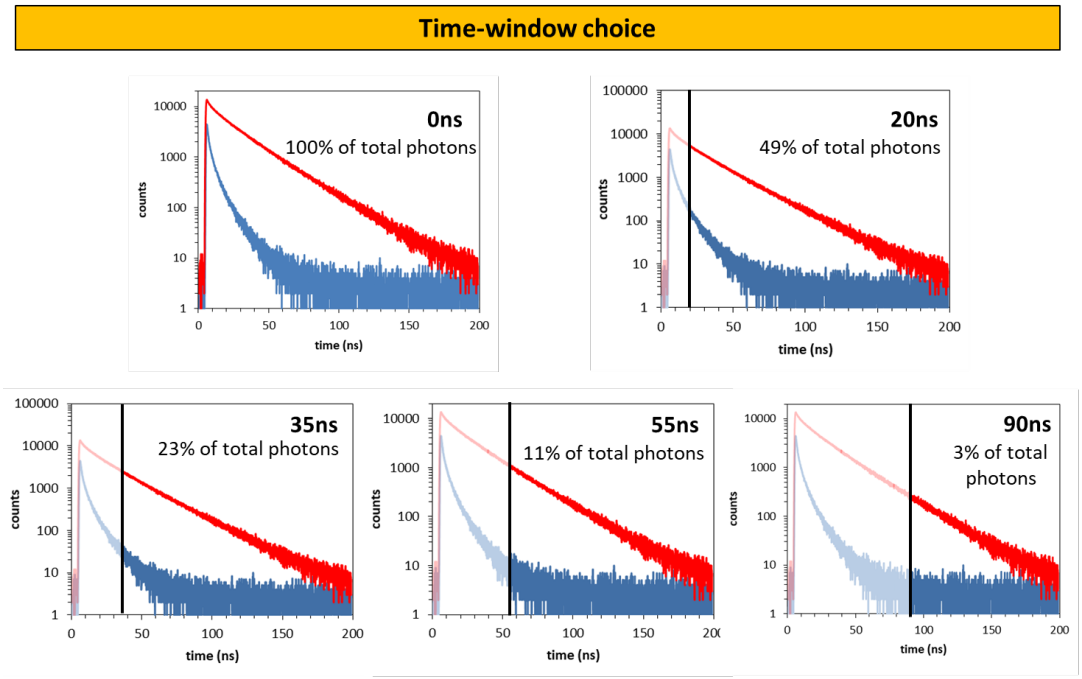


**Figure S5.** Fluorescence decay traces from Q-Sph (blue) and PNA122*/miR-122 duplex adsorbed on Q-Sph beads (red). Different time-windows are applied to the histograms.

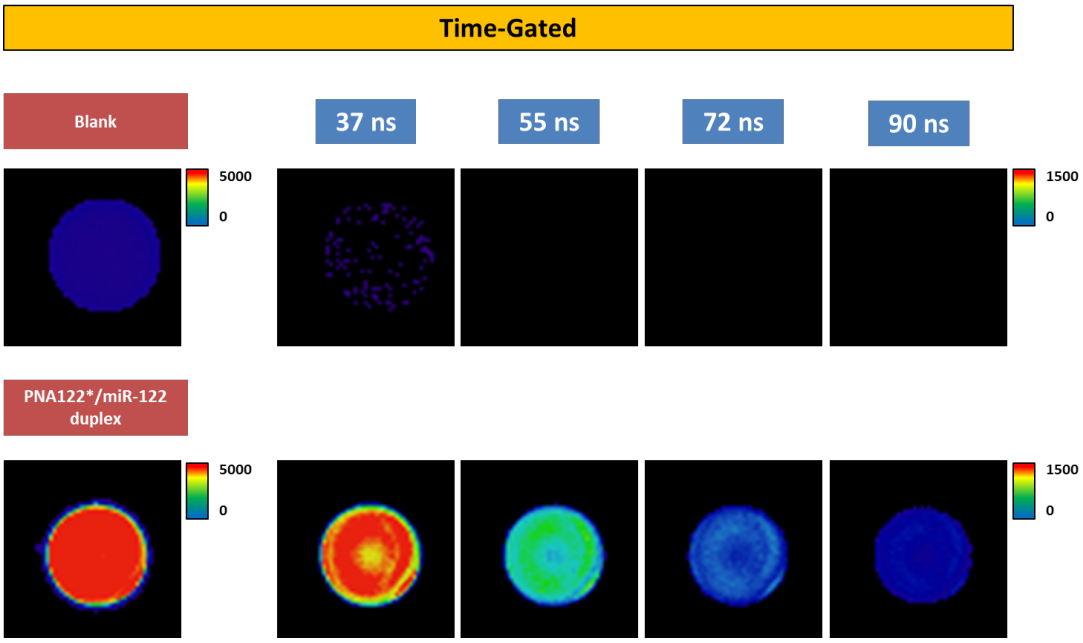


**Figure S6.** TG intensity images from (top) a single Q-Sph bead and (bottom) a Q-Sph bead in the presence of PNA122*/miR-122 duplex. Four different detection time-windows were applied: 35 ns, 55 ns, 72 ns and 90 ns. Images size is 80x80 $\mu m^2$.

In order to accurately estimate the best time-window choice, we have also performed a simulation for a DCL-TGI assay comparing the decay curves for a solution of target miR-122/DGL122/SB-C* duplex (solution 1) and a blank Q-Sph solution (solution 0). Signal-to-noise (S/N) function was calculated dividing smoothed intensity of solution 1 over solution 0 for each time, figure S7. Results show that this S/N ratio is maximized for times 40-90 ns when decay

curve of solution 0 starts to drop to residual counts. According to the first derivative of S/N function, figure S7, the maximum signal-to-noise ratio is achieved for time ca. 55ns, which is in agreement with data of figures S5 and S6.

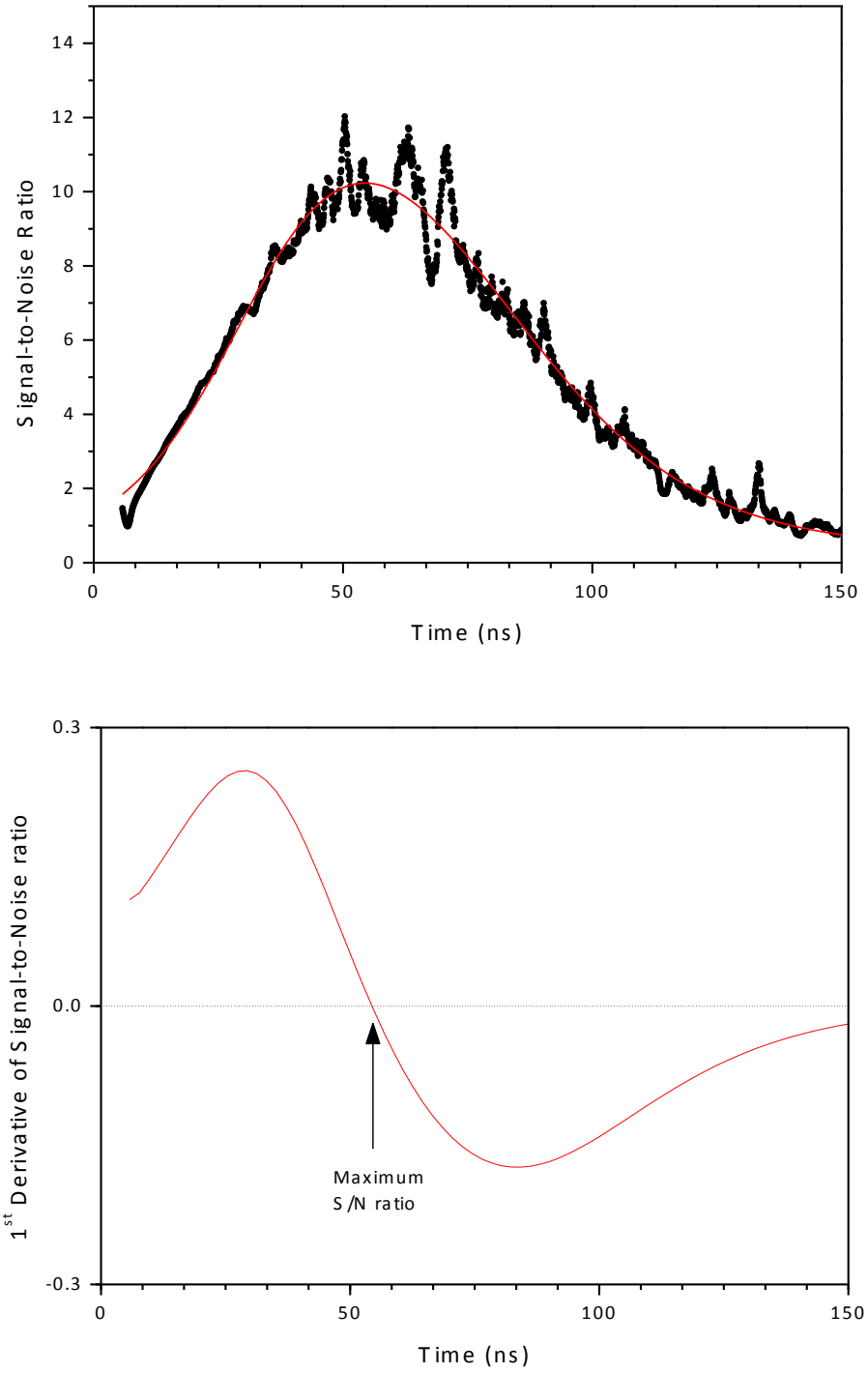


**Figure S7.** (top) Signal-to-Noise ratio of intensity decays of figure S5 solutions at different times (black points), red lines is the smoothed S/N function after fitting it to an asymmetric double sigmoidal function. (bottom) First derivative of signal-to-noise ratio showing the point of maximum S/N ratio.

### E2.6. Treatment of human serum samples

Serum samples were studied using the DCL-TGI assay, as referred in section E2.2 and Chart 1 in the main text of the manuscript, but with some modifications due to the nature of real human serum samples. In a first step (a), 10µL of serum sample were treated with 25µL of lysis buffer, 7.5µL of DGL122 (13µM) and water for a final volume of 45µL. This was kept reacting for 60 minutes at 30°C and agitation at 1200 r.p.m. In a second step (b), this sample was mixed during 30 minutes at 41°C with 1µL of SB-C* (500 µM), 3µL of $NaBH_3CN$ (5mM) and phosphate buffer pH 6 for a final volume of 100 µL. Later, solution was separated with the minimum possible amount of Q-Sph (15-20 beads) and led to the microscope. For miR-122 spike-in experiments, desired concentrations of miR-122 were added to step (a) instead of water and followed to step (b) as previously described.

# RESULTS

## R1. Spectral characterization and chemical stability of SeTau425 and derivatives

### R1.1. SeTau425

Absorption, excitation and emission spectra of SeTau425 are shown in figure S8. SeTau425 is characterized by a long Stokes shift (ca. 125 nm) with maxima in its UV-Vis absorption spectra at 340 nm and 425 nm and a single emission band at 542 nm in water. This compound has an average fluorescence lifetime of ca. 25 ns (Fig. S12 and Table S3) and a fluorescence quantum yield around 0.39 (free dye). This dye shows good chemical stability and its excitation and emission spectra and lifetimes do not show significant changes with pH between 2 and 7. The dye is also stable at conditions employed in this work, including the incubation at 41°C in the presence of the reducing agent $NaBH_3CN$. The addition of miR and PNA/miR duplexes to SeTAu425 did not lead to important changes, neither in its absorption, emission spectra or fluorescence lifetime. This suggests that there is no direct interaction, such as intercalation, between the SETau425 dye and the nucleic acids used in this work, at the experimental working conditions.

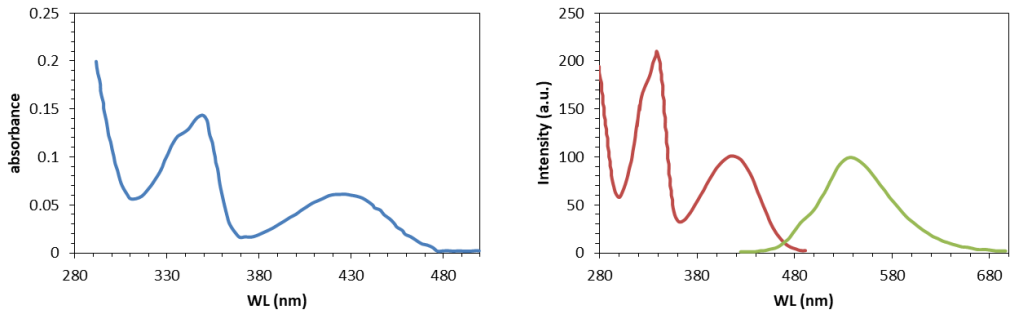


**Figure S8.** (left) Absorption, and (right) excitation ($\lambda_{em}$ = 550 nm) and emission spectra ($\lambda_{exc}$ = 425 nm) of SeTau425 in phosphate buffer, pH 6.0.

### R1.2 PNA122*

When the SeTau425 dye was incorporate to the PNA122* probe, via covalent bond, and the corresponding hybridized PNA122*/miR-122 duplex, it showed similar photophysical features than the free SeTau425 in solution. A slight decrease in the Stokes shift was detected due to a bathochromic effect on the absorption and a hypsochromic effect on the emission spectra (Fig. S9). The fluorescence lifetime of the dye spanned between 22-25 ns, after functionalization of the PNA122 and hybridization with miR-122 (Fig. S12 and Table S3).

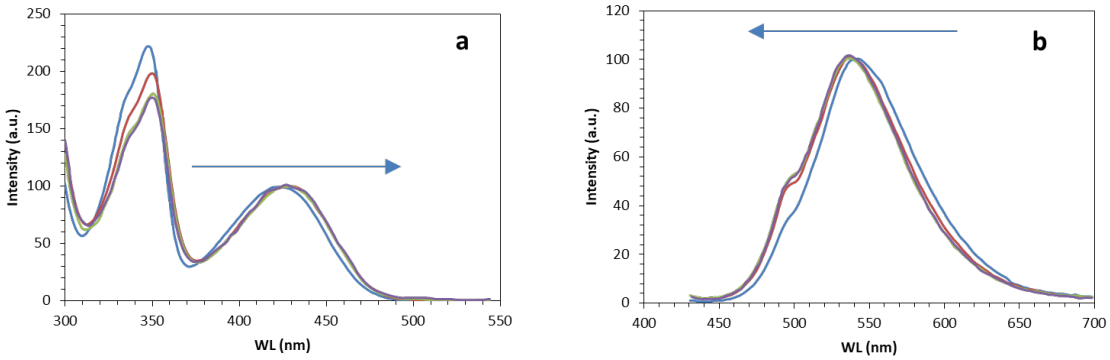


**Figure S9.** Normalized fluorescence (a) excitation spectra ($\lambda_{em}$ = 550 nm) and (b) emission spectra ($\lambda_{exc}$ = 425 nm) of free SETau425 (blue line), PNA122* (red), PNA122*/miR-122 duplex (green), and PNA122*/miR-122-18A duplex (purple). Arrows indicate the shift of the band.

## R1.3. SB-C*

Absorption spectra of SB-C* can be considered as the sum of bands from two contributions: the SMART Base (SB) core and the SeTau425 moiety (figure S10). Thus, excitation of SB-C* at wavelengths above the SB absorption (350nm) showed strictly the emission profile of the SeTau425 dye. Likewise, the excitation spectra collected at the emission wavelength of 550 nm only showed excitation of the SeTau425 dye. This confirms that there is no energy transfer process from the base core to the fluorescent dye.

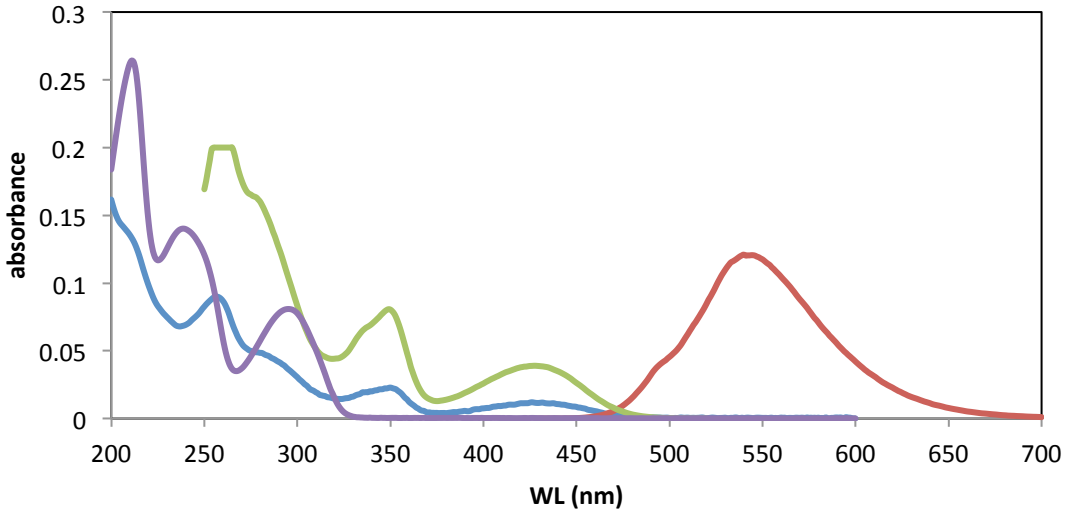


**Figure S10.** Absorption (blue line), excitation ($\lambda_{em}$ = 550 nm) (green line) and emission ($\lambda_{exc}$ = 425 nm) (red line) spectra of SB-C*. For comparison, the absorption spectra of the SB (purple line) is also shown.

A small decrease in the fluorescence intensity was observed in the SeTau425 dye label after performing the hybridization, dynamic incorporation of the SB-C* base, and subsequent covalent linkage by reduction with $NaBH_3CN$ (Fig. S11). However, the reduced SB-C* was still fluorescent enough, keeping the same spectral properties of SB-C* and the free SETau425. Furthermore, the lifetime of SeTau425 in the incorporated SB-C* remained within the 22 ns

range. Therefore, even after this reaction, the dye still keeps good spectral and photophysical characteristics to act as long-lifetime fluorescent reporter.

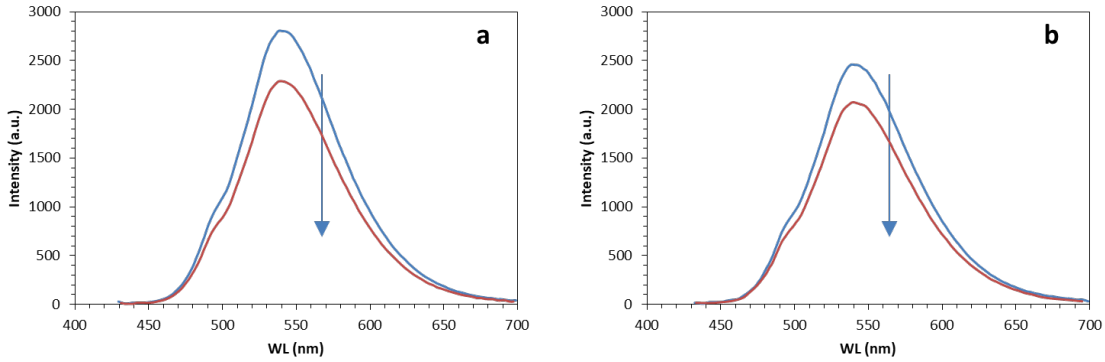


**Figure S11.** Emission spectra ($\lambda_{exc}$ = 425 nm) of SB-C* in phosphate buffer, pH 6.0. (a) SB-C* before (blue) and after (red) reduction treatment with $NaBH_3CN$. (b) SB-C* treated with $NaBH_3CN$ (blue) and miR-122-18G/DGL122 (red).

## R1.4. Time-resolved fluorescence spectroscopy of SeTau425, PNA122* and SB-C*

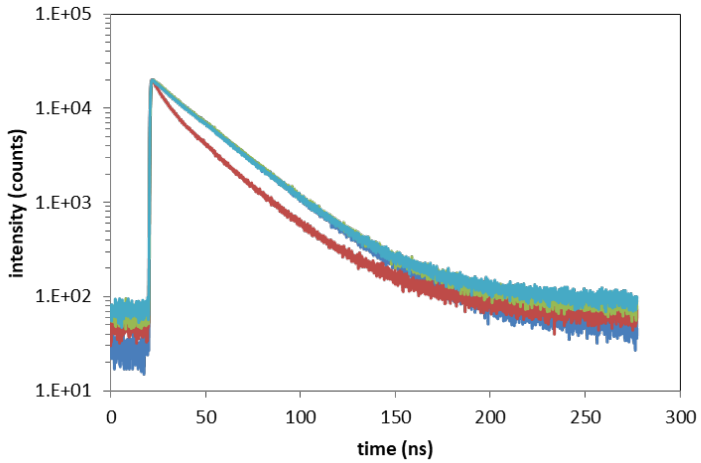


**Figure S12**. Fluorescence decay traces of free SETau425 (blue line), PNA122* (red), PNA122*/miR-122 duplex (green), and PNA122*/miR-122-18A duplex (cyan), with $\lambda_{exc}$ = 405 nm and $\lambda_{em}$ = 550 nm.

**Table S3.** Average fluorescence lifetimes, <τ>, of SeTau425 free in solution and labelling the nucleic acid strands used in this work.

| Sample | <τ> /ns[a] |
|---|---|
| **SeTau425-NHS** | 25.64 |
| **PNA122*** | 21.25 |
| **PNA122*/miR-122** | 25.61 |
| **PNA122*/miR-122-18A** | 25.42 |

[a] The average lifetimes were obtained from global analyses of three different decay traces, collected at 540, 550, and 560 nm, after pulsed excitation at 405 nm.

## R2. Photophysical and TGI imaging controls with Q-Sph beads

### R2.1. Q-Sph beads autofluorescence

We carried out the characterization of the autofluorescence emission of Q-Sph beads with FLIM imaging, to measure both the emission intensity and lifetime. We observed weakly fluorescent beads, of tens of microns of diameter (Fig. S13). The fluorescence decay traces from these images followed multi-exponential decay functions, with an average lifetime of ca. 4 ns. This fluorescence may come from scattering of excitation light and autofluorescence of the materials that constitute the Q-Sph beads.

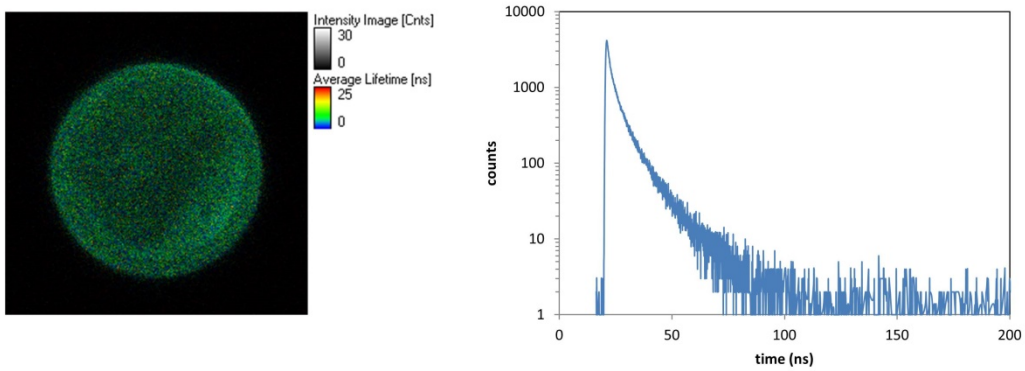


**Figure S13.** 80x80 $\mu m^2$ FLIM image of a Q-Sph bead suspended in phosphate buffer, pH 6.0; and the corresponding overall fluorescence decay trace obtained from the image.

### R2.2. Unspecific adsorption and autofluorescence from miRs, DGL122, and PNA122*

We have also checked other eventual autofluorescence sources, which might cause interferences in the detection protocol. We have investigated the emission from the labelled PNA122* probe, the unlabelled miR-122 and the miR-122/DGL122 duplex adsorbed on Q-Sph beads at common working concentrations (Fig. S14). FLIM images of the Q-Sph beads exhibited lifetime components of ca. 1, 4, and 12 ns, similar to those obtained for bare Q-Sph particles. No significant contribution from miR-122 or DGL122 to the TGI images appeared under these conditions, as the TGI filtering removed most of the fluorescence from the particle, as expected. Similar results were obtained from a solution of PNA122*, meaning that this probe does not interact with Q-Sph beads at the working concentrations.

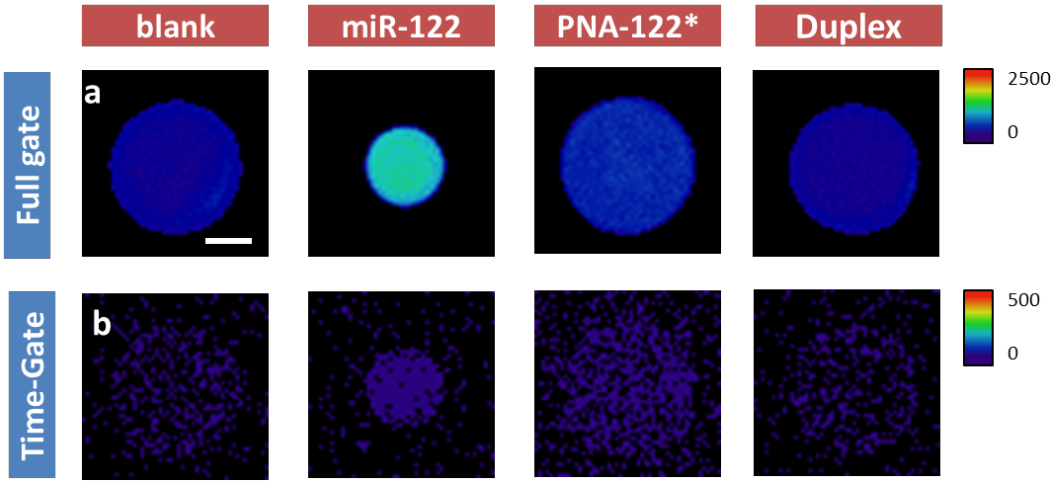


**Figure S14.** Intensity images of Q-Sph beads in a blank solution, and in the presence of 1 µM miR-122, 1 µM PNA122* or 1 µM of the DGL122/miR-122 duplex. Full window (a) and TGI-filtered images (b, 55 ns time window) are shown. Colour scales indicate emission intensity.

## R2.3. Unspecific adsorption of SB-C* on Q-Sph beads

A potential source of interference in our DCL-TGI assay would be the unspecific adsorption of the labelled SB-C* base on the bead. This would prevent the actual identification of the duplex, since free, unreacted SB-C* may remain on the bead, even after the washing steps. Hence, as a control, we checked the potential adsorption of SB-C* on Q-Sph beads with both steady-state fluorescence measurements and FLIM imaging.

Should this interaction happens, the addition of Q-Sph beads to a solution of SB-C* would decrease the fluorescence intensity, since SB-C* molecules would be retired from bulk solution to the bottom of the cuvette upon deposition of the beads. Importantly, we did find a negligible decrease of the intensity after a first treatment with Q-Sph (Fig. S15). Excitation spectra showed similar results. Therefore, we can confirm that Q-Sph beads are not significantly adsorbing SB-C* molecules, thus the dye remains in the bulk solution.

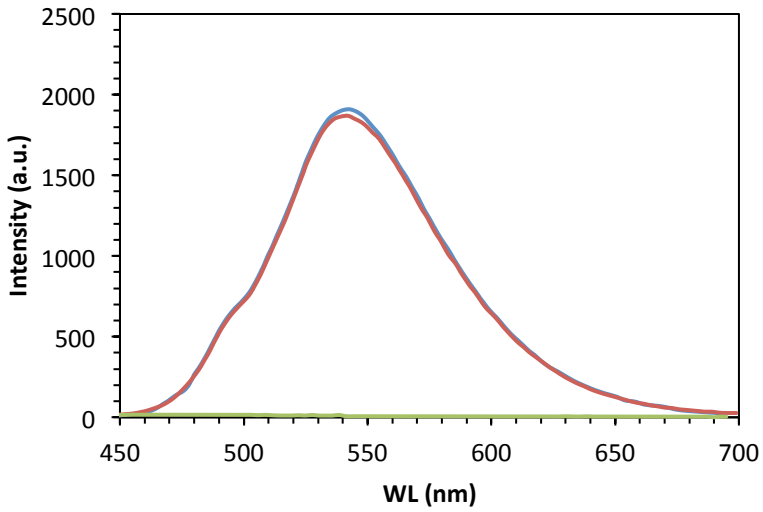


**Figure S15.** Emission spectra ($\lambda_{exc}$ = 425 nm) of SB-C* in solution before (blue) and after (red) the addition of Q-Sph beads. The emission spectrum of a blank solution, only containing Q-Sph beads, is also shown (green line).

We have also incubated two different concentrations of SB-C* (50 nM and 5 µM) with Q-Sph beads, and imaged them in the FLIM and TGI imaging without further separation (Fig. S16). At low SB-C* concentration, the TGI image was similar to a blank solution. No significant fluorescence from the dye is localized over the particle in the full-gated image, nor in the TGI image, meaning that the long component of SeTau425 in the SB-C* was not present. For high concentrations of the SB-C* base, 5 µM (results not shown), the full-gated image showed homogeneity outside the Q-Sph bead, from SB-C* in the bulk solution, but even lower emission intensity in the area of the particle, in agreement with its more inaccessible nature. Consistently, the TGI image also showed less intensity in the area of the particle, and we did not observe a higher concentration of SB-C* over the beads in relation to the bulk.

All these experiments allowed to draw the conclusion that free SB-C* bases do not represent a source of potential interferences in the DCL-TGI assay, due to unspecific adsorption on the Q-Sph beads.

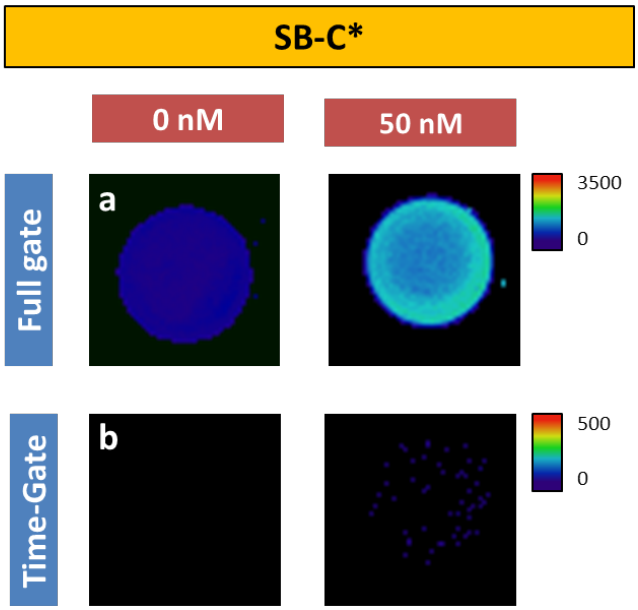


**Figure S16.** Intensity images of Q-Sph (left) and Q-Sph + SB-C* 50 nM (right) in phosphate buffer, pH 6.0, at different detection time-windows: (a) Full-gated, and (b) 55-ns TGI-filtered images. Images size is 80x80 $\mu m^2$.

## R2.4. Controls of unspecific interactions of SB-C* with other reagents

We have checked separately the potential interaction of the SB-C* base with each component of the DCL-TGI assay to rule out other possible sources of interferences. We have investigated the interaction of SB-C* with the individual miR-122 and DGL122 strands, not forming the duplex, and with the miR-122/DGL122 duplex but without the presence of the reducing agent that promotes the covalent binding of the base within the interrogation *pocket*. Results in Figure S17 evidence that significant amounts of long-lived photons from SeTau425 are not detected in any case. The TGI images showed some intensity when the SB-C* base is present, due to transient diffusion of the labelled base, but homogeneously found in solution and surrounding the bead. It is worth noting that even in the presence of the miR-122/DGL122 duplex, under non-reducing conditions, the adsorption of SB-C* was not detected. This means that the reducing agent, $NaBH_3CN$, is necessary for a permanent insertion of SB-C* to the duplex. In this case, a slightly higher intensity was found in the surroundings of the particle, possibly due to the transient dynamic binding/unbinding events of SB-C* within the duplex pocket. Importantly, emission from the SB-C* base is unequivocally and exclusively detected when it is incorporated according to the full protocol. These negative controls are in clear contrast with the positive results shown in the main text.

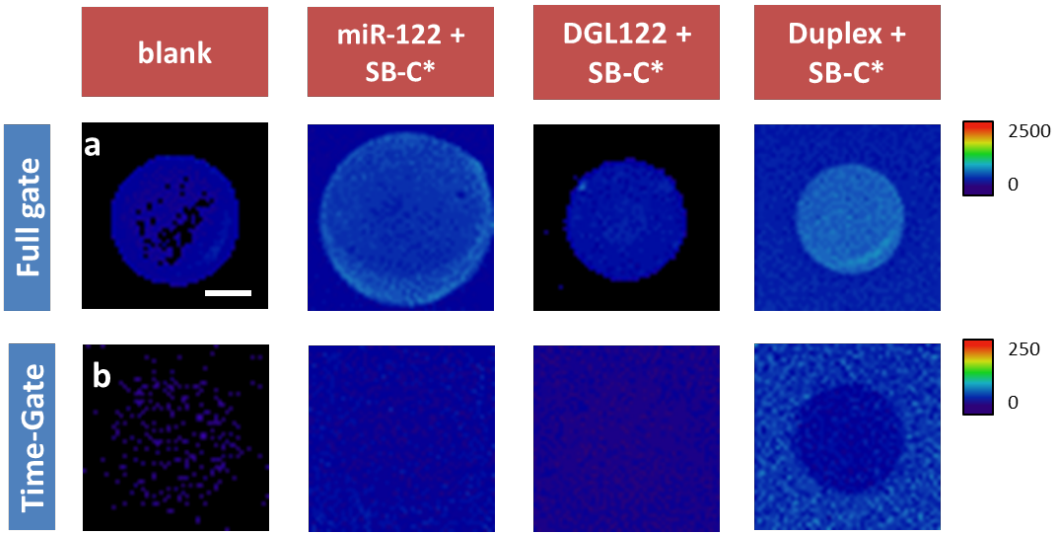


**Figure S17.** Intensity images of Q-Sph beads in a blank solution, and in the presence of miR-122 1µM + SB-C*, DGL122 1µM + SB-C*, and DGL122/miR-122 duplex 1µM + SB-C*, at different detection time-windows: (a) Full window, and (b) TG-filtered (55ns) images. Colour scales indicate emission intensity.

## R2.5. Nature of the interaction between Q-Sph beads and the nucleic acid complexes

The addition of NaCl 1M to the Q-Sph beads containing the full SB-C*/DGL122/miR-122 duplex exhibited a clear release of some of the fluorescence to the bulk solution (Fig. S18). The release of labelled duplex demonstrates the electrostatic nature of the interaction with the Q-Sph beads.

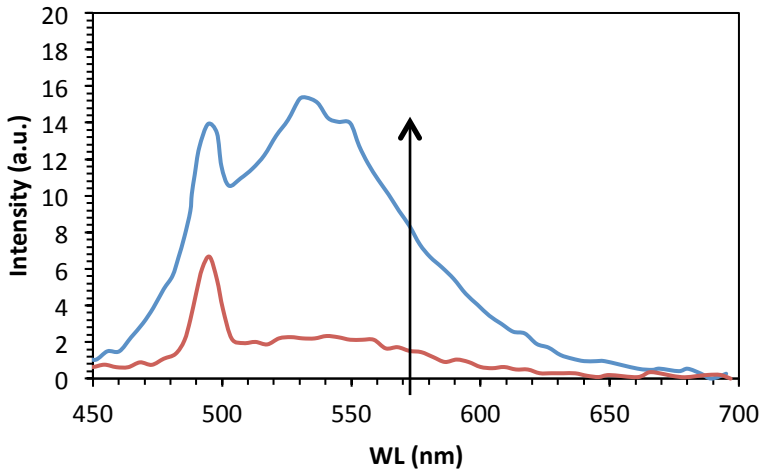


**Figure S18.** Emission spectra ($\lambda_{exc}$ = 425 nm) of SB-C*/DGL122/miR-122 duplex solution (after DCL-TGI assay) before (red line) and after (blue line) the addition of NaCl 1M.

## R3. Optimization of the duplex adsorption on the Q-Sph beads

Duplex per bead ratio and incubation time are two key points for a better detection of target miR. We improved the detection reducing the number of available beads by directly selecting just one single bead (see Chart S2) and performing a kinetic study of the adsorption of PNA122*/miR-122 over the Q-Sph beads (Fig. S19). For this purpose, we placed a diluted solution of Q-Sph on a microscope slide. Visualization of the beads through the optical microscope helped to pick a single bead using aspiration with a micropipette. This bead was led to the confocal microscope and deposited over the slide which contained 10 µL of a 10 nM solution of PNA122*/miR-122 duplex. Immediately after, we registered FLIM and TGI images continuously during 90 min. Results are shown in Figure S19. Strikingly, this figure shows how the bead surroundings underwent an enhancement in the fluorescence emission intensity (and average lifetimes, not shown) with time. This is especially noticeable in the TGI images, indicating the presence of the SeTau425 dye, corresponding to further loading of the duplex PNA122*/miR-122. According to these results, we established an incubation time of at least 50 min for the adsorption of the formed duplexes on the bead surface when single-bead approach is performed.

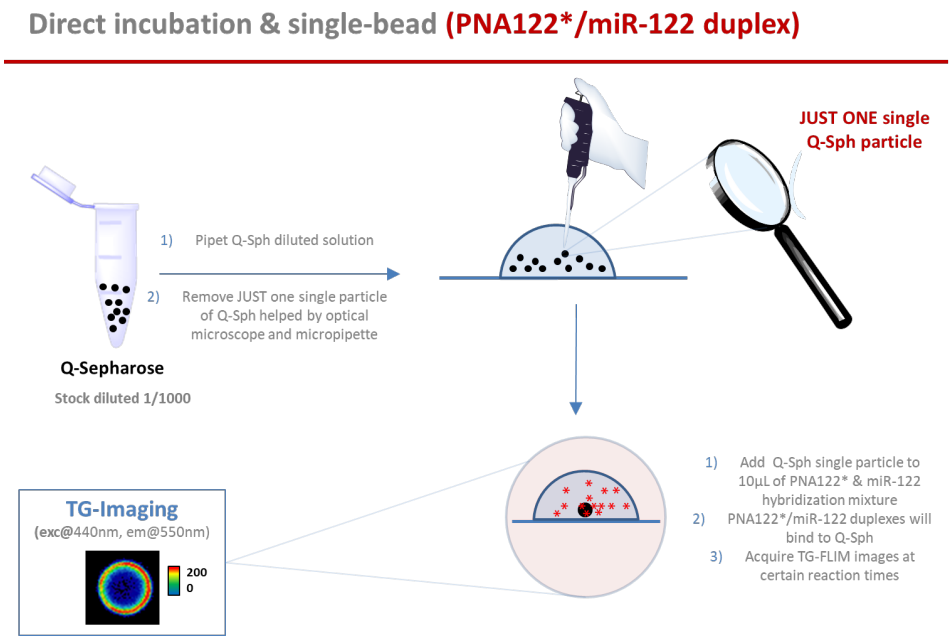


**Chart S2.** Procedure for the selection of just one single bead, subsequent incubation with PNA122*/miR-122 and acquisition at the confocal microscope.

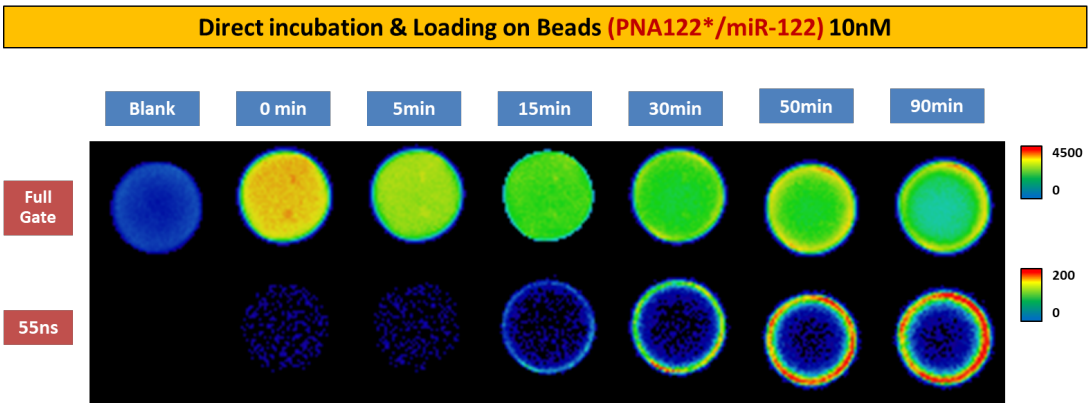


**Figure S19.** Full-gated and TGI (55ns window) intensity images of a Q-Sph bead in the presence of PNA122*/miR-122 10 nM at different incubation times. Colour scales indicate emission intensity.

## R4. Optimization of the excitation laser power in PNA122*/miR-122 methodology

We have performed several experiments to detect different concentrations of labelled duplex, ranging over 5 order of magnitude, under the PNA122*/miR-122 methodology. One of the inconveniencies found in working with such broad range was the saturation of the single photon detectors when the emission intensity was too high. Figures S20 and S21 show full-gated and TGI intensity images, respectively, from PNA122*/miR-122 duplex samples, with concentrations ranging from 1 µM to 100 pM. As expected, for samples with the lowest concentrations we needed to increase the excitation power of the laser. However, high laser powers caused saturation on the detector with samples of higher concentrations. Hence, the excitation power is another key point for detection of low amounts of duplexes. Under these high power conditions, we could clearly distinguish 1 nM duplex samples from blank solutions. As shown in figure 1 of the main text, further improvement in the limit of detection was achieved by increasing the acquisition time-per-pixel. Although this method increases the time for the analysis, one can unequivocally detect concentrations as low as 100 pM of duplex (Fig. 1 in main text).

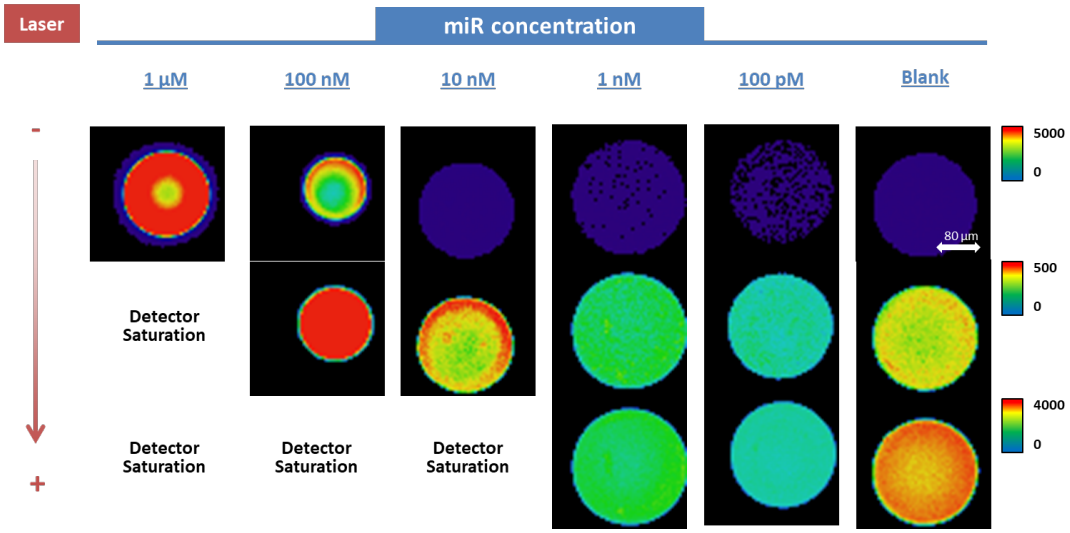


**Figure S20.** Full-gated intensity images of Q-Sph beads with PNA122*/miR-122 duplex solutions at different concentrations (100 pM – 1 µM), and different excitation laser powers, compared with a blank solution. Colour scales indicate emission intensity.

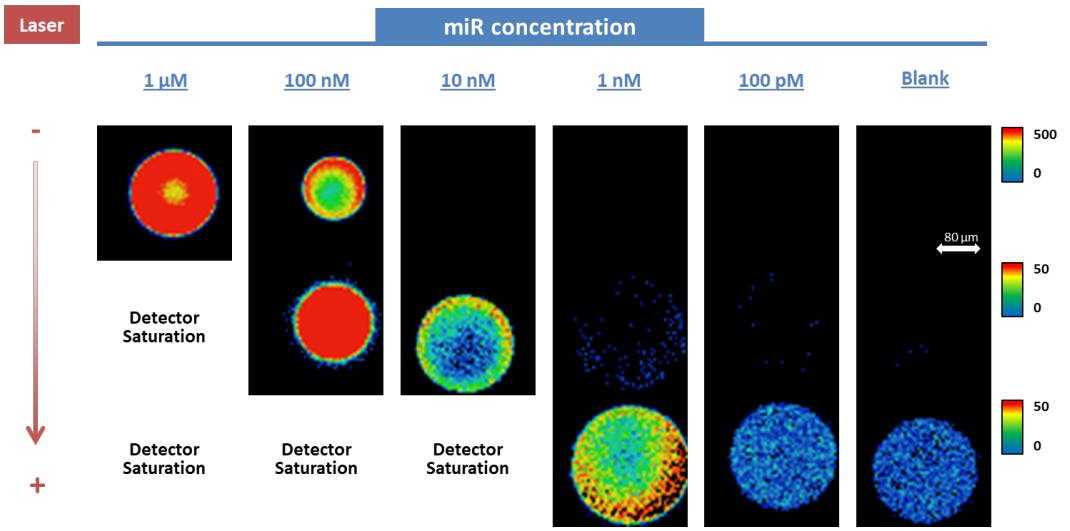


**Figure S21.** TGI intensity images (55-ns time window) of Q-Sph beads with PNA122*/miR-122 duplex solutions at different concentrations (100 pM – 1 µM) and different excitation laser powers, compared with a blank solution. Colour scales indicate emission intensity.

## R5. Optimization of the time-gating window for the DCL-TGI assay

Using the DCL-TGI assay, we can differentiate single point mutations in the miR-122 sequence, as shown in figure 2 in the main text. The advantage of using a complete FLIM analysis is that different time windows can be tested and optimized. Figure S22 shows the full-gated and TGI images, using different gating windows, for the sequences miR-122, miR-122-22G, and miR-122-18A, analysed using the DCL-TGI assay; this is the hybridization with the DGL122 probe and the incorporation of the labelled SB-C* base. Figure S22 clearly shows that the best signal-to-noise ratio is achieved with a 55-ns time window, which is in agreement with previous data of figure S7.

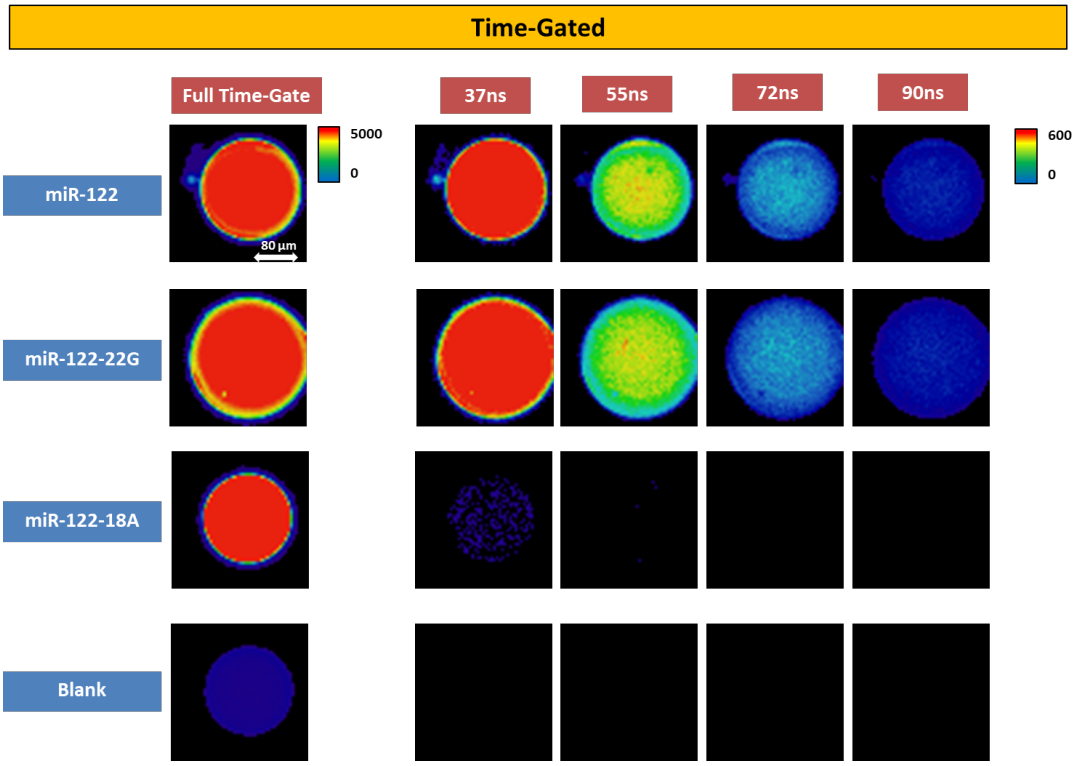


**Figure S22.** TGI intensity images of Q-Sph beads in the presence of miR-122, miR-122-22G, and miR-122-18A (1 µM), analysed with the DCL-TGI assay (with DGL122 and SB-C*). Colour scale indicates emission intensity.

## R6. DCL-TGI assay applied to the detection of miR-122 in human serum samples

### R6.1. Controls with bovine serum albumin

We carried out some control experiments with the bovine analogue of human serum albumin (HSA) to determine possible sources of interference in the hybridization reaction of the DCL-TGI assay, since blood serum contains a huge variety of molecules with different chemical binding abilities, e. g., sugars, substrates, electrolytes and proteins (emphasizing serum albumin), just to mention some of them. These components feature different chemical binding abilities and may cause some kind of disruption in proper functioning of the methodologies proposed here due to unspecific binding.

For example, we tested the hybridization reaction in the presence of Bovine Serum albumin (BSA) at 0.4% (w/V), finding a negligible increase in the intensity of Q-Sph beads that vanishes after applying TGI filtering. Therefore, no relevant differences in the performance of the miR-122 detection were found in presence of BSA (Figure S23).

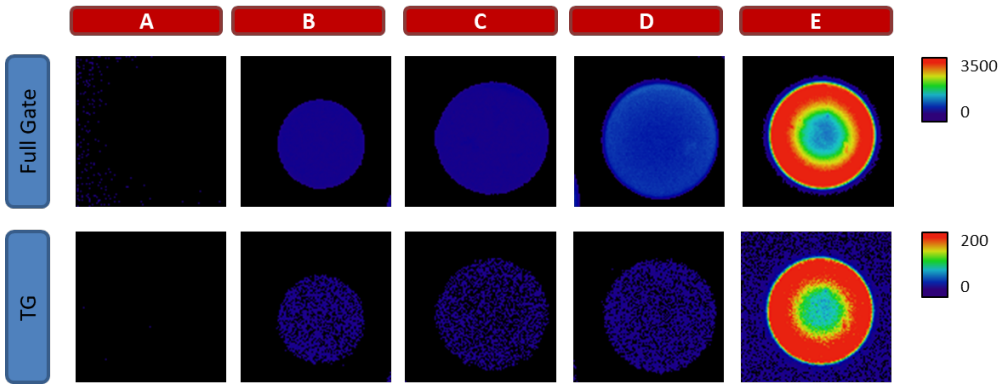


**Figure S23.** Effect of BSA in the performance of the DCL-TGI assay. Full window and TGI-filtered (55ns) intensity images of Q-Sph beads in (A) a blank solution, and in the presence of (B) SB-C* 5µM, (C) SB-C* 5µM + DGL122 1µM, (D) SB-C* 5µM + miR-122 1µM, (E) full reaction: SB-C* 5µM, DGL122/miR-122 duplex 1µM. All the samples contain 0.4% (w/V) of BSA. Colour scales indicate emission intensity.

## R6.2. Spike-In test on control human serum samples

To test the detection capabilities towards miR-122 and the limit of detection of the DCL-TGI assay in serum samples, we employed a control, commercial human serum and a total concentration of 100 pM of miR-122 was spiked in (2 femtomoles of miR-122 in 20 μL of human serum). We compared the obtained signal with the background noise obtained from the untreated serum solution (blank), SB-C* in serum solution, and DGL122 and SB-C* in serum solution as controls. The latter experiment would be representative of a complete DCL-TGI assay applied to a serum in which the miR-122 levels are negligible. Indeed, our results showed some background signal in those control experiments that are attenuated when TGI filtering is applied. In any case, significantly distinguishable signal is obtained between the sample containing 100 pM of spiked-in miR-122 and that in the absence of miR-122 (Fig. S24).

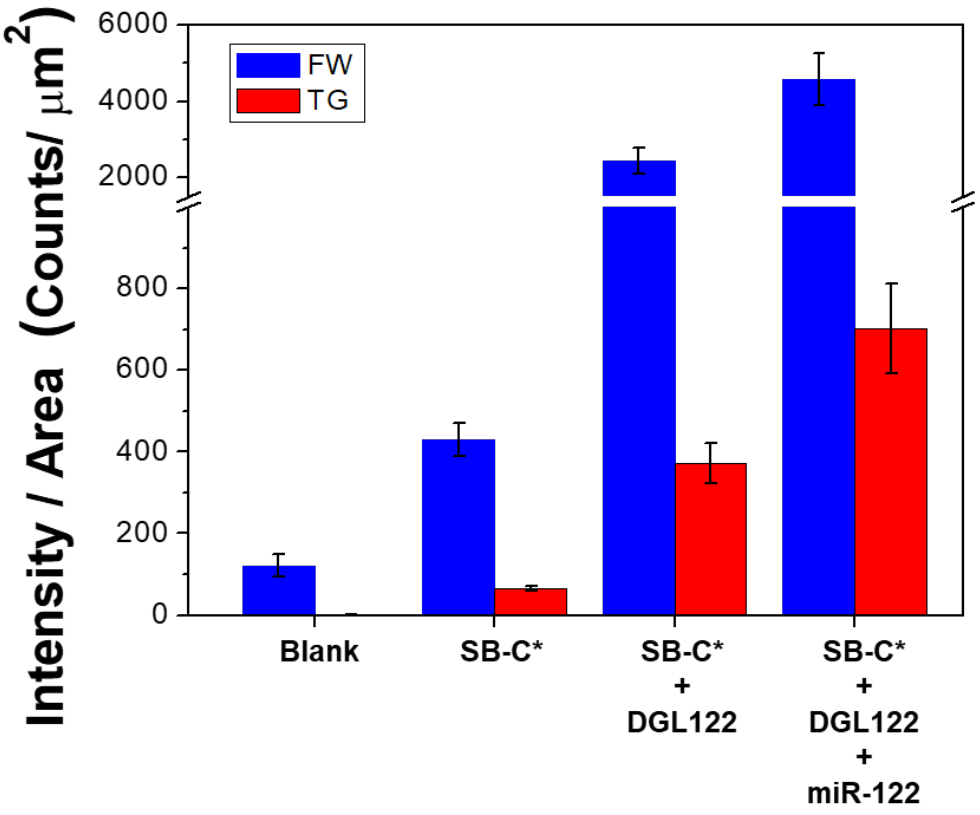


**Figure S24.** Intensity per area of Q-Sph beads obtained from intensity images of control serum solution (blank), and in presence of SB-C* 5 μM, SB-C* 5 μM + DGL122 1 μM, and the full DCL-TGI assay (SB-C* 5μM, DGL122 1 μM + miR-122 100 pM). The different detection time-windows are shown: (blue) Full window, and (red) TGI-filtered (55ns) images.

### R6.3. Statistical analysis of the results of the DCL-TGI assay applied to human serum

We performed DCL-TGI assays of control human serum and serum from a DILI patient (triplicated measurements of four different aliquots each, for a N = 12 in each sample). The results of average intensity per area unit were related to the minimum value for a control serum measurement (Fig. S25). Statistical, non-parametric test for two independent samples (NPH-TS, Mann-Whitney test) was performed to validate the hypothesis that the two populations, control and DILI patient, are significantly different. Our results show that the two populations are statistically different, with a confidence level of 96%, using the DCL-TGI assay. Using a full-gate analysis, which would be comparable to conventional microscopy techniques, resulted in very similar results, although the confidence level for validating the hypothesis decreased down to 93%.

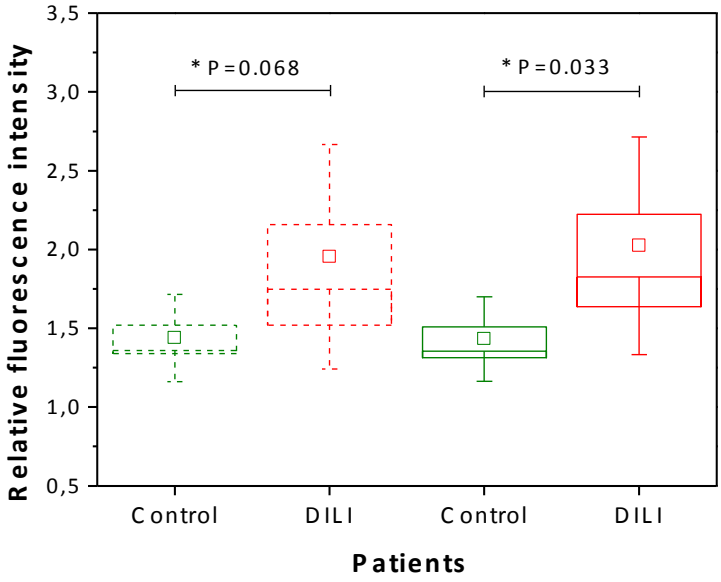


**Figure S25.** Box plot of the relative average fluorescence intensity in DCL-TGI assays, using full-gate (dashed boxes) or TGI-filtering (solid boxes), of a control human serum samples (N = 12, green) and a DILI patient serum samples (N = 12, red). Boxes and whiskers represent the standard error and standard deviation, respectively. Square symbols and horizontal line represent the average and median, respectively. Non-parametric statistical Mann-Whitney test of the data confirmed the two populations are different at 0.93 confidence level (full-gate, $p$ = 0.068) or 0.97 confidence level (TGI-filtered, $p$ = 0.033).

# ESI references


1. F. R. Bowler, J. J. Diaz-Mochon, M. D. Swift, and M. Bradley, *Angew. Chem. Int. Ed. Engl.*, 2010, **49**, 1809–1812.

2. M. Bradley and J. J. Diaz-Mochon, 2009.

3. J. W. Dear, J. I. Clarke, B. Francis, L. Allen, J. Wraight, J. Shen, P. I. Dargan, D. Wood, J. Cooper, S. H. L. Thomas, A. L. Jorgensen, M. Pirmohamed, B. K. Park, and D. J. Antoine, *Lancet Gastroenterol. Hepatol.*, 2018, **3**, 104–113.

4. B. López-Longarela, E. E. Morrison, J. D. Tranter, L. Chahman-Vos, J.-F. Léonard, J.-C. Gautier, S. Laurent, A. Lartigau, E. Boitier, L. Sautier, P. Carmona-Saez, J. Martorell-Marugan, R. J. Mellanby, S. Pernagallo, H. Ilyine, D. M. Rissin, D. C. Duffy, J. W. Dear, and J. J. Díaz-Mochón, *BioRxiv*, 2019.

5. J. Schindelin, I. Arganda-Carreras, E. Frise, V. Kaynig, M. Longair, T. Pietzsch, S. Preibisch, C. Rueden, S. Saalfeld, B. Schmid, J.-Y. Tinevez, D. J. White, V. Hartenstein, K. Eliceiri, P. Tomancak, and A. Cardona, *Nat. Meth.*, 2012, **9**, 676–682.